Nonradiative recombination and its influence on the lifetime distribution in amorphous silicon (*a*-Si:H)

Ruben Stachowitz, Meinolf Schubert, and Walther Fuhs
Fachbereich Physik und Wissenschaftliches Zentrum für Materialwissenschaften, Philipps Universität Marburg, D-35032 Marburg, Germany
(Received 10 May 1995)

We present a detailed analysis concerning the influence of the defect density N_D on the low-temperature ($T=10$ K) geminate recombination kinetics. It is shown that the lifetime distribution of *a*-Si:H, measured by frequency-resolved photoluminescence spectroscopy, can be explained quantitatively if it is assumed that radiative recombination is directly competing with nonradiative tunneling into defect states. This allows us to determine the radiative lifetime distribution with high accuracy, which in turn provides the unique opportunity to describe the recombination kinetics entirely, i.e., including its nonradiative contribution. Interesting and nonintuitive consequences that are related to the competition model are discussed.

I. INTRODUCTION

It is well known that hydrogenated amorphous silicon (*a*-Si:H) gives rise to photoluminescence (PL) of high efficiency at low temperatures. PL experiments thus provide an effective tool for studying the recombination kinetics in this material, detecting a substantial part of the excess carrier population. The lifetime distribution of the photogenerated carriers has been shown to be of particular interest,[1–19] and most of the recombination models were derived on the basis of this quantity. There are two experimental techniques commonly used for lifetime measurements: time-resolved spectroscopy (TRS) and quadrature frequency-resolved spectroscopy (QFRS). While TRS records the PL decay, following a short laser pulse, QFRS measures the 90° phase-shifted frequency response under stationary excitation conditions. Though equivalent in theory, it seemed as if the two methods were producing conflicting results. Based on TRS data Tsang and Street[19] derived the geminate-pair model, according to which the recombining electron-hole pairs are correlated, being created in the same absorption process. The QFRS data,[3,6,8] however, seemed to indicate that there is no such correlation, which led to the distant-pair model,[7] where it is proposed that electrons and holes are randomly distributed in space. This problem, which arises due to the accumulating background carrier concentration in the band tails[20] was finally resolved, and it was shown by Bort *et al.*[4] that geminate recombination is also observable with QFRS, once the generation rate is decreased below the critical value $G_0 \sim 5\times10^{18}$ cm^{-3}s^{-1}. There is, however, another important issue where a discrepancy between TRS and QFRS data has remained. This concerns the question of whether the nonradiative channel introduced by the defects is actually directly competing with luminescence, affecting both quantum efficiency *and* radiative recombination kinetics. At first glance it appears as if this question should be easy to answer, since, in the case of direct competition, the decrease of the PL quantum efficiency is usually expected to correspond to a proportional decrease of the observed lifetime [see Eqs. (4) and (5) in Sec. III B]. However, while Tsang and Street[18] find that the fast contribution to the PL decay becomes much more significant with increasing defect density N_D, the observed shift of the QFRS lifetime spectra seems to be comparatively small.[3] It therefore appears as if TRS is pointing towards direct competition, while QFRS is implicating just the opposite.

In this paper it is shown that the QFRS data are in complete accordance with the concept of a directly competing nonradiative recombination channel. This is done quantitatively, giving a detailed analysis of how the recombination kinetics are influenced in the presence of this channel. The analysis allows us to derive the lifetime distribution for the defect-free case, revealing that the fast radiative process in the microsecond range is in fact intrinsic and not defect related. This result is particularly interesting and contrary to the view of Searle *et al.*[11] and Boulitrop and Dunstan,[21] who attributed the origin of this process to a competing nonradiative channel. Finally, it is demonstrated that measuring the quantum efficiency η_{PL} as a function of N_D may not be sufficient for deciding whether competition is involved, and it is shown that the TRS decay data may be misleading as well, if not carefully analyzed.

II. EXPERIMENTAL DETAILS AND RESULTS

The experiments were performed at $T=10$ K in a standard FRS setup using light of 1.96-eV photon energy. The modulation depth was kept at approximately 15% of the bias light, with a constant generation rate $G=3\times10^{17}$ cm^{-3}s^{-1}, which is sufficiently low to ensure geminate excitation conditions. The defect density was varied by electron bombardment (2 MeV, 4 K) and successive annealing between $T=300$ and 470 K in the range $N_D=1.7\times10^{16}$–5.5×10^{17} cm^{-3}. N_D was determined after each annealing step by the constant photocurrent

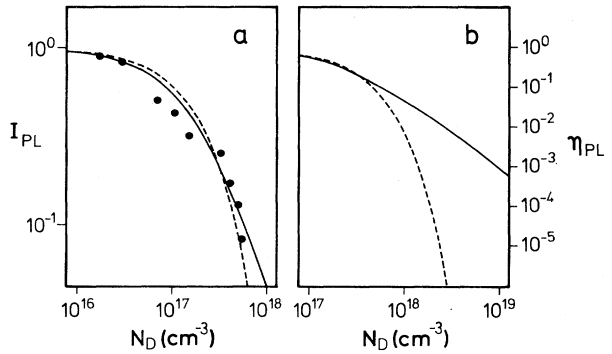

FIG. 1. (a) Relative luminescence intensity I_{PL} for various defect densities N_D, at $T=10$ K. Solid and dashed lines are theoretical predictions, calculated according to Eqs. (12) and (17), respectively. For details see Sec. III C. (b) Same as in (a), but on different scales.

method (CPM spectroscopy).

Figure 1(a) shows the familiar dependence of the relative luminescence intensity I_{PL} on N_D; whereas I_{PL} is nearly independent of the defect density for $N_D < 3\times10^{16}$ cm^{-3}, it decreases rapidly once N_D exceeds 10^{17} cm^{-3}. The scatter of the data is remarkably small as compared to data which are obtained if the defect density is varied by changing the deposition parameters such as rf power, substrate temperature, silane concentration, etc.[22] However, in that case every single value for I_{PL} corresponds to a different sample with different properties, while the data in Fig. 1(a) [and Fig. 2(a)] were obtained on only one sample. Varying the defect density by electron bombardment is therefore preferable, especially if the data are to be analyzed quantitatively.

In Fig. 2(a) it is shown how the QFRS lifetime spectra

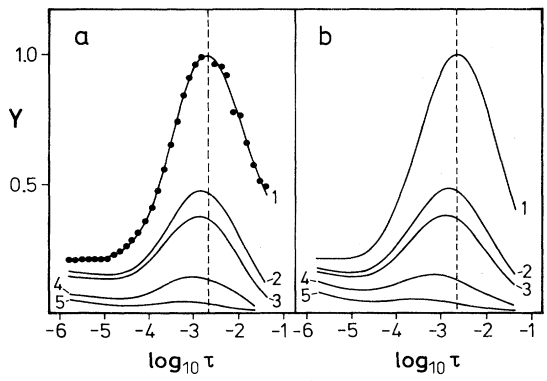

FIG. 2. (a) QFRS spectra for various defect densities N_D, at $T=10$ K. (1) $N_D=1.7\times10^{16}$ cm^{-3}, (2) 7×10^{16} cm^{-3}, (3) 1.1×10^{17} cm^{-3}, (4) 3.2×10^{17} cm^{-3}, (5) 5.5×10^{17} cm^{-3}. The full circles are the original data points for curve 1. (b) Theoretical QFRS spectra, calculated according to Eq. (6). (1) $N_D=1.7\times10^{16}$ cm^{-3}, (2) 1.3×10^{17} cm^{-3}, (3) 1.7×10^{17} cm^{-3}, (4) 3.3×10^{17} cm^{-3}, (5) 5.6×10^{17} cm^{-3}. Details are given in Sec. III B.

change with increasing defect density. For low values of N_D the spectra are only weakly dependent on the defect density, consisting of the pronounced and well-known "geminate peak" at $\tau\sim2$ ms and a plateau that extends into the microsecond range (curve 1). Then, corresponding to the decreasing luminescence intensity, the signal amplitude is quenched in the entire time domain and the spectra are systematically shifted towards shorter lifetimes. The shift, however, is smaller than what is expected from the decrease in I_{PL}, and this was considered to be evidence for a model according to which the defects introduce a nonradiative but noncompeting recombination channel.[3] On the other hand, a closer look at the spectra reveals that longer lifetimes are quenched much more effectively than faster processes, eventually leading to a situation where the geminate peak is no longer dominating the spectrum (curve 5). This result, again, is quite typical for a competing nonradiative process that becomes faster as the defect density increases. Part of the following discussion is to show that the defects indeed introduce a directly competing nonradiative recombination channel.

III. DISCUSSION

A. General considerations

As mentioned in the previous section, it is well known that the steady-state luminescence intensity I_{PL} is independent of the defect density once the latter is decreased below a value of $N_D\sim3\times10^{16}$ cm^{-3}, irrespective of the preparation conditions for the samples.[22] It further has been shown that I_{PL} is independent of temperature for $T<50$ K, provided that the generation rate G is low enough to ensure geminate conditions;[23,24] this is not the case for high G, where $I_{PL}(T)$ reveals a pronounced maximum at $T=50$ K.[19] There is, however, an uncertainty concerning the question as to whether the quantum efficiency η_{PL} is unity under these conditions (low N_D, low T) or is intrinsically limited to some value $\eta_0<1$.[25] Principally, it is of course important to know the true value of η_0 because this determines if there are other nonradiative processes at low temperatures besides the one which is introduced by the defects. Nevertheless, this issue is of minor importance for the problem of how the recombination kinetics are influenced by the latter. The following analysis is thus restricted to nonradiative recombination via defects, and for reasons of simplicity it is assumed that $\eta_0=1$.

B. Radiative and nonradiative recombination kinetics

The purpose of this section is twofold. First, it is shown that the nonradiative channel, introduced by the defects, is indeed directly competing with the radiative channel. This is done quantitatively by deriving an analytical expression for the QFRS signal and subsequently comparing calculated and experimental spectra (see Fig. 2). The second part is then concerned with the analysis of this competing mechanism and with the question of how the recombination kinetics—including its

nonradiative contribution—are affected by it.

For low temperatures and geminate generation rates the PL in a-Si:H is linearly dependent on the excitation such that the rate of change of the excess carrier density, following a short laser pulse, can be described as a superposition of exponentials:

$$\frac{dn}{dt}=\text{const}\times\int_0^\infty G(\tau)\frac{1}{\tau}\exp(-t/\tau)d\tau\ . \tag{1}$$

G is the probability density for the generation of an electron-hole pair with lifetime τ and is usually called the lifetime distribution. Since this decay contains both radiative and nonradiative transitions, G consists of two contributions as well, i.e., $G=G_r+G_{\rm nr}$. The radiative part of the decay, $I_{\rm PL}(t)$, is therefore given by

$$I_{\rm PL}(t)=\text{const}\times\int_0^\infty G_r(\tau)\frac{1}{\tau}\exp(-t/\tau)d\tau\ . \tag{2}$$

The QFRS signal $Y(\omega)$ is now easily derived by applying linear-response theory, from which it follows that it is basically given by the sine Fourier transform of $I_{\rm PL}(t)$ (Ref. 26) that

$$Y(\omega)=\text{const}\times\int_0^\infty G_r(\tau)\frac{\omega\tau}{1+\omega^2\tau^2}d\tau\ . \tag{3}$$

As stated above, it is assumed that the detected luminescence (described by G_r) results from two directly competing recombination channels, one being strictly radiative and the other one strictly nonradiative. It is further assumed that the lifetimes of the two competing channels can be treated like statistically uncorrelated variables with distribution functions P_r and $P_{\rm nr}$, respectively. Consequently, every recombination step is characterized by a particular pair of lifetimes τ_r and $\tau_{\rm nr}$, where the actual time constant τ of the transition is given by

$$\tau^{-1}=\tau_r^{-1}+\tau_{\rm nr}^{-1}\ . \tag{4}$$

The probability σ for the transition to be radiative is a function of τ_r and $\tau_{\rm nr}$ as well, and it is obtained by

$$\sigma=\frac{\tau_r^{-1}}{\tau_r^{-1}+\tau_{\rm nr}^{-1}}\ . \tag{5}$$

Note that σ must not be confused with $\eta_{\rm PL}$, since there are more than just two values for τ_r and $\tau_{\rm nr}$ and thus $\eta_{\rm PL}$ is given by the ensemble average $\langle\sigma\rangle$ [see Eq. (12)]. With knowledge of P_r and $P_{\rm nr}$, G_r can be determined via Eqs. (4) and (5), which allows us to subsequently calculate the QFRS signal according to Eq. (3). As far as the latter is concerned, however, it is more convenient to modify Eq. (3) such that the dependence of the signal on P_r and $P_{\rm nr}$ is given explicitly, thereby avoiding the numerical calculation of G_r. This is readily achieved by substituting τ via Eq. (4) and by replacing G_r by the corresponding distribution function for the two respective lifetimes. Since τ_r and $\tau_{\rm nr}$ are assumed to be uncorrelated, this function is given by the product $P_r\times P_{\rm nr}\times\sigma$, where the factor σ accounts for the fact that only radiative transitions are detected. Averaging over all possible lifetime configurations then yields the QFRS signal. There are,

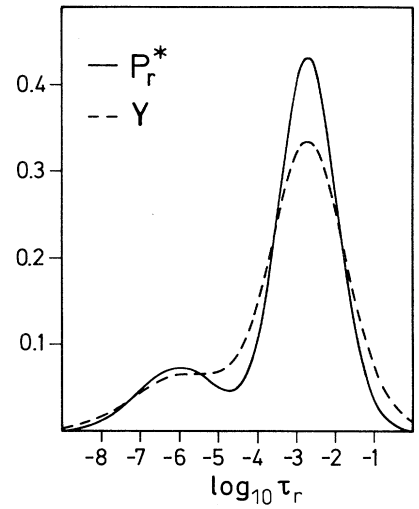

FIG. 3. The radiative distribution function P_r^* according to Eq. (11) and the corresponding QFRS signal.

however, two reasons why this transformation should be carried out with respect to the logarithmic lifetime variables and their corresponding distribution functions, denoted by P_r^* and $P_{\rm nr}^*$, rather than referring to the linear variables. The first reason is that the QFRS signal has been shown to give a good approximation for G_r^*, the distribution function of $\log_{10}\tau$, provided that G_r^* is sufficiently broad.[14,15] This indeed holds true for a-Si:H, where G_r^* is known to extend over several orders of magnitude in time[4,19] (see also Fig. 3, later in this section, where the accuracy of the approximation is nicely demonstrated). This interesting feature is particularly useful, for it follows that the observed changes in the QFRS spectra, which are consequently plotted as a function of $\log_{10}\tau=-\log_{10}\omega$, directly reveal how G_r^* is affected in the presence of the nonradiative channel, sparing the necessity of further data reduction. The second reason is that the nonradiative tunneling model[18] is in fact closely related to $P_{\rm nr}^*$, which makes it especially easy to interpret the observed changes in terms of the proposed model. With respect to these considerations and using the substitutions $x_r=\log_{10}\tau_r$, $x_{\rm nr}=\log_{10}\tau_{\rm nr}$, and $z=\log_{10}\omega$, one then obtains for the QFRS signal

$$Y(z)=\text{const}\times\int_{-\infty}^{\infty}\int_{-\infty}^{\infty}P_r^*(x_r)P_{\rm nr}^*(x_{\rm nr})\sigma(x_r,x_{\rm nr})\times\frac{10^z/(10^{-x_r}+10^{-x_{\rm nr}})}{1+10^{2z}/(10^{-x_r}+10^{-x_{\rm nr}})^2}\times dx_r dx_{\rm nr}\ . \tag{6}$$

This equation presents the basis for the analysis of the quadrature signals shown in Fig. 2(a), and in principle it should be appropriate for every system where radiative and nonradiative recombination are directly competing.

The next step is to determine the distributions P_r^* and $P_{\rm nr}^*$, after which the predictions of Eq. (6) can be compared with the experiment. However, while $P_{\rm nr}^*$ is deter-

mined analytically according to the model proposed by Tsang and Street,[18] P_r^* will be derived on the basis of the experimental data alone. This approach seems to be mandatory, since, so far, it has not been possible to obtain the radiative distribution for geminate excitation conditions on theoretical terms.[14,15,27]

In order the explain the dependence of the quantum efficiency η_{PL}, and in particular the dependence of the PL decay on the defect density, Tsang and Street[18] suggested that the dominant nonradiative process at low temperatures is the competing tunneling transition of a trapped band-tail electron into a defect state. For an electron surrounded by N defects at separations $R_1, R_2, .., R_N$, the transition rate τ_{nr}^{-1} is then given by total recombination rate

$$\tau_{nr}^{-1}=\nu_0 \sum_{i=1}^{N} \exp(-2R_i/\alpha) , \tag{7}$$

where $\nu_0 \sim 10^{12}$ s^{-1} has the value of a typical phonon frequency and where the localization length of the electron was estimated to be $\alpha \sim 10-12$ Å.[16,19] It can be shown, however, that for all practical purposes it is sufficient to consider only the separation between the electron and the *nearest*-lying defect, which is due to the strong exponential dependence of the respective rates on R_i.[28] Equation (7) therefore reduces to the familiar expression

$$\tau_{nr}^{-1}=\nu_0 \exp(-2R/\alpha) , \tag{8}$$

from which it follows that the nonradiative distribution is solely determined by the distribution function for the nearest-neighbor distances, $H(R)$. If the defects are randomly distributed in space, as is usually assumed, then $H(R)$ is given by[29]

$$H(R)=4\pi R^2 N_D \exp(-4\pi R^3 N_D/3) . \tag{9}$$

This distribution is basically identical with P_{nr}^*, since $dR \equiv \frac{1}{2}\alpha \ln 10\, d \log_{10}\tau_{nr}$, and with $R(\log_{10}\tau_{nr}) = \frac{1}{2}\alpha \ln 10(\log_{10}\tau_{nr}+\log_{10}\nu_0)$ one obtains

$$P_{nr}^*(x_{nr})=\tfrac{1}{2}\alpha \ln 10 H(R(x_{nr})) . \tag{10}$$

The radiative distribution is determined on the basis of the QFRS data shown in Fig. 2(a). This is achieved by selecting one of the spectra and fitting it with Eq. (6), where P_r^* is now the only unknown quantity. Of course, this approach depends on the assumption that the nonradiative channel is indeed directly competing and correctly described by Eq. (10). It is, however, subsequently justified by the agreement which is obtained for the calculated and the recorded signals. At any rate, taking a curve from the low defect-density range ensures that any possibly falsifying impact of the proposed model is minimized, because nonradiative recombination is then of minor importance. Hence, P_r^* was determined by fitting curve 1 ($N_D=1.7\times10^{16}$ cm^{-3}), using the parameters $\nu_0=10^{12}$ s^{-1} and $\alpha=11$ Å. According to the result that the plateau in the microsecond range is related to a second intrinsic radiative process,[14,15] it was started out with a superposition of two Gaussians for P_r^* and indeed one obtains a very good fit for

$$P_r^*(x_r)=0.431 \exp[-0.89(x_r+2.7)^2] + 0.072 \exp[-0.45(x_r+6)^2] . \tag{11}$$

This distribution is given by the solid line in Fig. 3. Since P_r^* is identical with G_r^* for $N_D=0$, we have also plotted the corresponding ($N_D=0$) quadrature signal, given by the dashed line. Further details concerning G_r^* are given later in this section.

Now that the two respective lifetime distributions have been determined, it is easy to calculate the QFRS signal for any given defect density via Eq. (6), where N_D remains as the only free fit parameter. Figure 2(b) shows the curves that give the best fit to the recorded signals and the agreement is indeed very good. The shift of the spectra is accurately reproduced, and the same holds true for the increasing quenching effect with increasing lifetime. It is also remarkable that the required values for N_D are very close to the experimentally determined values, the largest deviation being smaller than a factor of 2, which is well within the experimental uncertainty. This result is very convincing evidence for the full applicability of the nonradiative tunneling model, demonstrating that it allows for a quantitative analysis of the recombination kinetics at low temperatures. Yet, it should be noted that based on TRS data, Collins *et al.*[30] have proposed a model where the defects are considered to act as fast ($\tau_{nr}<10$ ns) and predominantly *noncompeting* recombination centers. The respective experiment was carried out at $T\sim80$ K and the PL was selectively detected for a single emission energy E_{PL}. Though the latter is uncritical at low temperatures ($T=10$ K) where G_r^* is only weakly dependent on E_{PL},[19,31] it is not for $T=80$ K, since the correlation between E_{PL} and the observed recombination kinetics is then quite strong.[31] Considering that the data of Collins *et al.* were obtained for an emission energy 250 meV above the steady-state luminescence peak energy, it thus seems questionable whether the recorded PL decays are indeed characteristic for the recombination kinetics of the excess carrier population. In addition, it must be taken into account that temperature itself introduces a nonradiative path for $T>50$ K (see, for example, Ref. 23). Obviously, the respective experimental results are difficult to compare, but nevertheless it can be stated that the model of Collins *et al.* is definitely not valid at low temperatures.

The good agreement between the measured and the calculated signals makes it seem worthwhile to take a closer look at some of the details concerning the lifetime distribution $G^*=G_r^*+G_{nr}^*$ and how it is affected in the presence of the two competing recombination channels. This is done in the following, starting with its radiative fraction G_r^*.

As mentioned above, G_r^* and P_r^* are identical for $N_D=0$, since recombination is then purely radiative. Figure 3 shows that this "intrinsic" lifetime distribution consists of two pronounced structures, the dominant geminate peak at $\log_{10}\tau_r=-2.7$ (2 ms) and a second peak centered at $\log_{10}\tau_r=-6$ (1 μs). The width of the former is approximately 1.8 decades and slightly smaller than the 2.5 decades for the faster process, the ratio of their

respective contributions to G_r^* being close to 4:1. The quadrature signals shown in Fig. 2 directly reveal how G_r^* evolves as the defect density increases, and, mainly, there are two effects that need to be discussed. Firstly, the distribution is shifted towards shorter times, which can be seen most clearly for the geminate peak; and, secondly, the ratio changes in favor of the μs process while the signal amplitude is quenched in the entire time domain. The interpretation of the latter is straightforward, since it follows from Eq. (5) that slow radiative processes are quenched stronger than faster ones, thus accounting for the changing ratio. The reason for the shift, on the other hand, is somewhat unexpected. Because it is correlated with an increase of the nonradiative rate (decreasing $\eta_{\rm PL}$), it seems natural to interpret the shift in terms of Eq. (4), in analogy to a system with only two single lifetimes τ_r and $\tau_{\rm nr}$, respectively. However, it turns out that the lifetime dependence of the quenching effect, as defined by Eq. (5), accounts for the shift as well. This shift is of a different type and similar to the effect that is obtained by multiplying a (bell-shaped) curve with a monotonously increasing or decreasing weight function; the respective peak positions of $\exp(-x^2)$ and $\arctan(x)\exp(-x^2)$, for example, being $x=0$ and $x=0.633$. We now show that the lifetime dependence of the quenching effect indeed accounts for virtually all changes in the QFRS signals shown in Fig. 2.

The reason for this feature is that, initially, when the quantum efficiency starts to decrease due to the rapidly decreasing pair-defect separations R, the major contribution to the PL nevertheless results from pairs where R is large, such that $\tau_r < \tau_{\rm nr}$ and hence $\tau \sim \tau_r$. Radiative recombination in the vicinity of "close" defects, which actually causes a shift of G_r^* in terms of Eq. (4), is only relevant for very high defect densities when the probability for these large values of R becomes negligible. This is readily verified by calculating the relative fraction of carriers, denoted by δ, that recombine radiatively yet without a shift of their respective lifetime τ_r. Since the quantum efficiency $\eta_{\rm PL}$ is given by

$$\eta_{\rm PL} = \int_{-\infty}^{\infty} G_r^*(x)dx = \int_{-\infty}^{\infty} P_r^*(x_r)\left[\int_{-\infty}^{\infty} P_{\rm nr}^*(x_{\rm nr})\sigma(x_r,x_{\rm nr})dx_{\rm nr}\right]dx_r \ , \tag{12}$$

δ is obtained as

$$\delta = \eta_{\rm PL}^{-1}\int_{-\infty}^{\infty} P_r^*(x_r)\left[\int_{x_r}^{\infty} P_{\rm nr}^*(x_{\rm nr})\sigma(x_r,x_{\rm nr})dx_{\rm nr}\right]dx_r \ . \tag{13}$$

Figure 4 shows these two quantities as a function of N_D, and it is to be seen that the increase of the nonradiative rate is not instantaneously followed by a shift of the PL lifetimes. Instead, δ remains in the order of unity for $N_D \lesssim 5\times10^{17}$ cm^{-3} and $\tau=\tau_r$ is thus a valid approximation in this range of N_D. This allows us to rewrite Eq. (6) in the following way:

$$Y(z) = \text{const}\times\int_{-\infty}^{\infty} P_r^*(x_r)\epsilon(x_r)\frac{10^{z+x_r}}{1+10^{2(z+x_r)}}dx_r \ , \tag{14}$$

where ϵ is defined by

$$\epsilon(x_r) = \int_{-\infty}^{\infty} P_{\rm nr}^*(x_{\rm nr})\sigma(x_r,x_{\rm nr})dx_{\rm nr} \ . \tag{15}$$

This definition is useful because it directly reveals the lifetime dependence of the quenching effect as described above: ϵ is the average probability for a pair with lifetime τ_r to recombine radiatively if it is located somewhere within the distribution of defects, and consequently ϵ decreases monotonously with increasing τ_r. This is demonstrated in Fig. 5, where ϵ is plotted for a defect

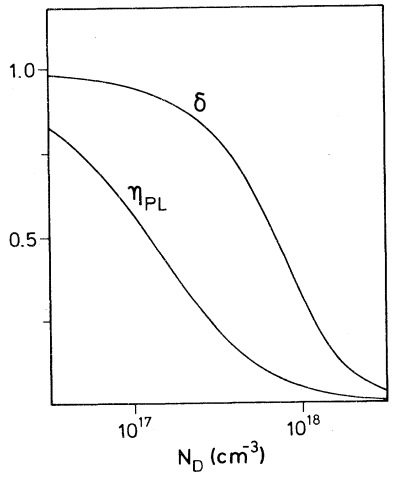

FIG. 4. The relative fraction δ of carriers with lifetime $\tau=\tau_r$ and the quantum efficiency $\eta_{\rm PL}$ as a function of N_D. The curves were calculated according to Eqs. (12) and (13).

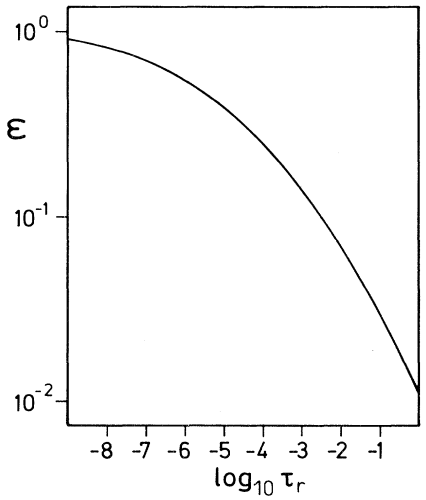

FIG. 5. The average probability ϵ for a pair with lifetime τ_r to recombine radiatively within a distribution of defects, calculated according to Eq. (15) for $N_D=3.3\times10^{17}$ cm^{-3}.

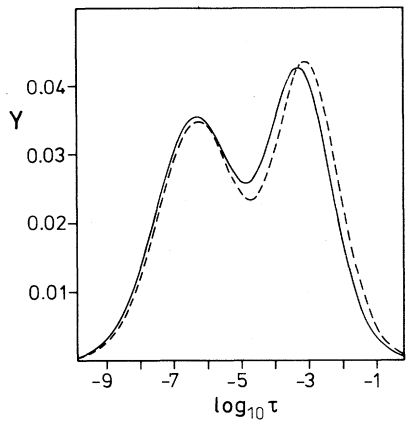

FIG. 6. QFRS signals, calculated according to Eq. (6) (solid line) and Eq. (14) (dashed line) for $N_D=3.3\times10^{17}$ cm^{-3}. The solid line is identical with curve 4, Fig. 2(b).

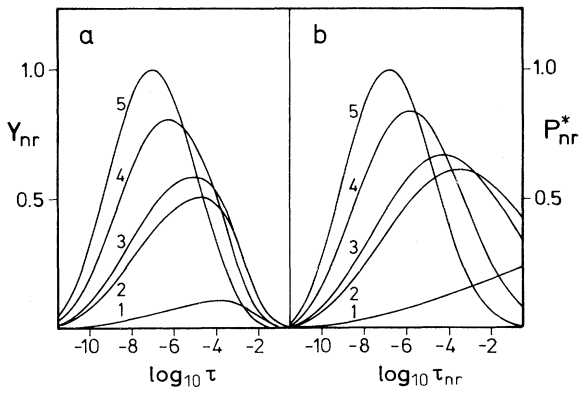

FIG. 7. (a) The nonradiative frequency response for various defect densities, calculated according to Eq. (6), where σ is replaced by $1-\sigma$. The values for N_D are identical with the ones in Fig. 2(b). (b) The corresponding nonradiative distributions P^*_{nr}, calculated according to Eq. (10).

density of $N_D=3.3\times10^{17}$ cm^{-3}. The comparison of Eqs. (3) and (14), on the other hand, shows that

$$G_r^*=\epsilon P_r^* \ , \tag{16}$$

and thus the changes in the QFRS signals of Fig. 2(a) must be predominantly an effect of the lifetime-dependent quenching. This is nicely illustrated in Fig. 6, where a QFRS signal calculated for $N_D=3.3\times10^{17}$ cm^{-3} via Eq. (6) (solid line) is shown, together with the respective approximation calculated via Eq. (14) (dashed line). Note that the marked influence of N_D on G_r^* is directly related to the fact that P_r^* is a broad and slowly varying function, since otherwise the modulation with ϵ would be ineffective. This means, however, that for systems with a narrow, δ-like distribution P_r^*, the initial decrease in η_{PL} will *not* be accompanied by a shift of the QFRS signals, which is quite a deceiving result, for it seems to indicate that the nonradiative channel is not competing with the radiative path.

Another important aspect of Fig. 6 is that it conclusively demonstrates that the origin of the μs process, which becomes more pronounced with increasing defect density, is completely independent of the defects. The most common point of view, according to which this structure is induced by the competition with a fast nonradiative channel (see, for example, Refs. 11 and 21), is therefore proven to be incorrect. This result is consistent with our recent analysis of low defect-density material,[14,15] where we have proposed that the fast process reflects the direct competition between radiative recombination and the final stages of thermalization, based on the result that the latter was shown to end in the μs range.[19] However, there might be other explanations concerning the true origin of this process, indicating that the issue requires further investigation.

A very interesting feature of the competition model is that it allows us to study the nonradiative kinetics quantitatively, since G^*_{nr} is determined by P_r^* and P^*_{nr} in exactly the same way as G_r^*. The only difference concerning the calculations is that the probability σ for a radiative recombination step has to be replaced by the probability for nonradiative recombination, which is simply $1-\sigma$. The easiest way to examine the influence of the defect density on G^*_{nr} is, thus, once again, to calculate the respective frequency response, denoted by Y_{nr}. Figure 7(a) shows the spectra that correspond to the ones which are shown in Fig. 2(b), being calculated for the same defect densities. The main difference between the two types of signals is evidently the strong shift of Y_{nr} with increasing N_D. This behavior is readily understood by studying the respective distributions of P^*_{nr}, which are plotted in Fig. 7(b). The cutoff of the signals in the ms range is obviously due to the competition with the radiative distribution P_r^*, which is a rapidly decreasing function for longer lifetimes, such that G^*_{nr} is virtually zero for $\log_{10}\tau>0$. For $\log_{10}\tau<-5$, on the other hand, G^*_{nr} is almost identical with P^*_{nr} since then in the vast majority of cases the effective lifetime is determined by the nonradiative process, the average logarithmic radiative lifetime being only -3.3. It follows that for high defect densities, when η_{PL} is small as compared to unity, the recombination kinetics will be entirely determined by P^*_{nr}, and therefore by the statistical distribution of the electron-defect separations. In the frame of the proposed model this is the expected result.

We now take a look at the quadrature signals, denoted by Y_S, which are obtained by superimposing the spectra of Figs. 2(b) and 7(a). It follows from $G^*=G_r^*+G^*_{nr}$ that these signals, shown in Fig. 8, reveal how G^* evolves as the defect density increases. For $N_D=1.7\times10^{16}$ cm^{-3}, Y_S resembles curve 1 in Fig. 2(a), reflecting the fact that recombination is predominantly radiative. For higher values of N_D the nonradiative contribution increases rapidly, although the radiative fraction is still clearly distinguishable for $N_D=1.7\times10^{17}$ cm^{-3}. Then, there is a rather drastic change in the kinetics such that for $N_D=3.3\times10^{17}$ cm^{-3} the remainder of the PL is merely

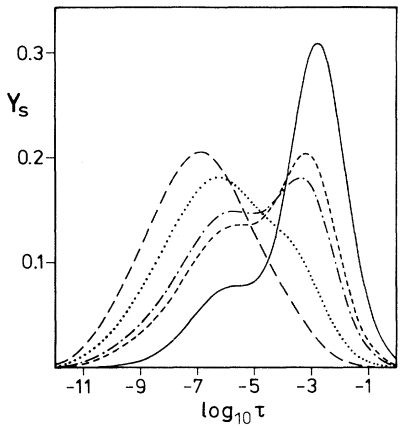

FIG. 8. QFRS signals, which are obtained by superimposing the signals of Figs. 2(b) and 7(a). For details see text.

recognizable as a small shoulder in the spectrum. For $N_D=5.6\times10^{17}$ cm^{-3} this shoulder has practically vanished and the kinetics are mainly determined by the nonradiative channel.

It should be emphasized at this point that the discussion of the distribution functions G^*_{nr} and G^* is not an academic construct. The competition model relates G^*_r and G^*_{nr} in an unambiguous way, making it sufficient to measure either one of the two quantities. Hence it is secondary that FRS is restricted to the radiative fraction.

C. The quantum efficiency

As shown in Sec. III B the quantum efficiency η_{PL} is easily calculated once the distribution functions P^*_r and P^*_{nr} have been determined. The respective prediction of Eq. (12), using the same values for ν_0 and α, is given by the solid line in Fig. 1(a). Again, the agreement with the experimental data is very satisfying. Peculiar, however, is the circumstance that the data can be described just as well by a noncompeting model. Street, Knights, and Biegelsen[22] found that the observed dependence of η_{PL} on N_D can be fitted by the well-known expression[18]

$$\eta_{PL}=\exp(-4\pi R_C^3 N_D/3)\ , \tag{17}$$

where R_C defines a critical capture radius for the defects. This is demonstrated by the dashed curve in Fig. 1(a), which corresponds to $R_C=105$ Å. However, although Eq. (17) was derived on the basis of an approximation within the competition model, it is in fact typical for a noncompeting recombination process. It assumes that every defect is surrounded by a sphere with volume $V_C=4\pi R_C^3/3$, representing a critical capture cross section: every electron-hole pair that is generated within such a sphere is captured in a nonradiative process, while it thermalizes and subsequently recombines radiatively if generated outside. In this case the quantum efficiency is identical to the probability of a pair being generated outside of a sphere V_C, which, depending on the defect density, is then given by Eq. (17). This sort of "direct capture" model is noncompeting by definition, since the decision as to whether a pair recombines radiatively or nonradiatively is independent of the respective lifetimes, decoupling the kinetics of the two recombination channels.

Figure 1(b) demonstrates that the two models are indeed quite difficult to distinguish for defect densities lower than $N_D=10^{18}$ cm^{-3}, but that they yield entirely different results for higher values of N_D (see also Refs. 9 and 28). While the noncompeting model leads to the strong exponential decrease of η_{PL}, competition predicts a considerably weaker dependence, close to a power-law behavior with exponent $\beta=-1.5$. In order to decide whether the η_{PL} data really indicate a competing nonradiative channel, it is therefore necessary to measure this quantity in the high defect-density range. However, for reasons given in the previous section, such an experiment needs to be carried out using an electron-bombardment sample. This was done by Street, Biegelsen, and Stuke,[32] and it is found that the dependence of η_{PL} on N_D is then indeed much weaker than exponential.

In this context it should be noted that TRS is confronted with a somewhat similar problem, making it difficult to decide whether the nonradiative channel is actually competing or not. It has been shown that the PL decay in *a*-Si:H consists of a fast and a slow component; the fast component becoming more significant with increasing N_D, while the slope of the slow decay remains virtually unaffected.[18] This behavior is generally considered to be *the* characteristic feature of a competing nonradiative recombination channel, which is correct if the radiative channel is governed by a single process. However, if there are (at least) two radiative processes separated in time, which, for instance, holds true in the case of *a*-Si:H, then it is possible to obtain very similar decay curves *without* competition being involved. This happens if only the slower of the two processes is quenched by the nonradiative channel, such that the increasing contribution at short times merely reflects the fact that the faster process remains uninfluenced. This interesting problem can be illustrated by calculating the *a*-Si:H decays with respect to both models. In case of competing recombination channels, the decay is obtained by the sine Fourier backtransform of Eq. (6), which leads to

$$I_{PL}(t)=\text{const}\times\int_{-\infty}^{\infty}\int_{-\infty}^{\infty}P^*_r(x_r)P^*_{nr}(x_{nr})10^{-x_r}\times\exp[-t(10^{-x_r}+10^{-x_{nr}})]\times dx_r dx_{nr}. \tag{18}$$

For the noncompeting situation, the decay is calculated via

$$I_{PL}(t)=\text{const}\times\int_{-\infty}^{\infty}G^*_r(x_r)10^{-x_r}\exp(-t10^{-x_r})dx_r\ , \tag{19}$$

where the radiative distribution and its dependence on N_D is given by

$$G^*_r(x_r)=P^*_{r1}(x_r)+\exp(-4\pi R_C^3 N_D/3)P^*_{r2}(x_r)\ . \tag{20}$$

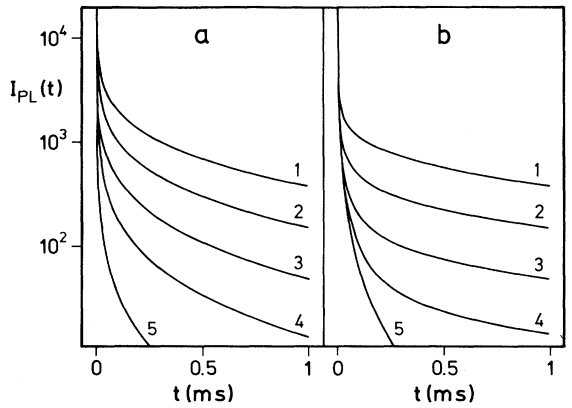

FIG. 9. (a) PL decays for competing recombination channels, calculated according to Eq. (18). (1) $N_D = 1.7\times10^{16}$ cm^{-3}, (2) 2×10^{17} cm^{-3}, (3) 4.3×10^{17} cm^{-3}, (4) 7×10^{17} cm^{-3}, (5) 1.2×10^{18} cm^{-3}. (b) PL decays for noncompeting recombination channels, calculated according to Eq. (19), using the same defect densities as in (a).

Here P_{r1}^* denotes the μs process while P_{r2}^* denotes the geminate peak, quenched by direct capture, again using the value $R_C = 105$ Å. Figure 9 shows the respective results, corresponding (a) to competition, and (b) to noncompetition. Indeed, both sets of data reveal the features of an increasing fast decay, while the slope of the slow component remains nearly N_D independent. As a matter of fact, competitive quenching of only the slower process would again yield curves that look very much the same. Nevertheless, there are some noticeable differences, making it possible distinguish between the different models if the data are quantitatively analyzed. The point is, however, that it is essential to be aware of the fact that the so-called "typical features" by no means provide unambiguous evidence for a competing nonradiative channel, and that there might be a problem where none is expected. In light of this, it should be considered an advantage of the QFRS technique that difficulties of this kind are avoided, since the spectra directly reveal how the radiative lifetime distribution G_r^* evolves as the defect density is changed.

IV. SUMMARY

In this paper we have shown that the competitive nonradiative tunneling model can quantitatively account for the QFRS lifetime spectra and their dependence on the defect density. This in turn allows us to determine the intrinsic ($N_D = 0$) geminate lifetime distribution with high accuracy, revealing that it consists of two clearly resolvable structures. In addition to the well-known geminate peak centered at $\tau \sim 2$ ms, there is a second one in the μs range, contributing to luminescence with approximately 20%. In contrast to the common and most intuitive view, it is shown that the increasing contributions to the QFRS signal at short times for increasing values of N_D, are in fact not induced by the competition between "slow" radiative and "fast" nonradiative transitions. Instead, it reflects that long radiative lifetimes are quenched more effectively than faster ones, such that the μs process emerges due to the suppressed geminate peak. An interesting feature of the presented analysis is that the nonradiative lifetime distribution may be studied concomitantly. This allows us to illustrate how the kinetics are changed in favor of the nonradiative channel as the quantum efficiency decreases, demonstrating that they are completely determined by the nearest-neighbor distribution for the pair-defect separations once N_D exceeds 5×10^{17} cm^{-3}. Analyzing the dependence of the quantum efficiency on N_D, it is shown that the competing nonradiative channel actually leads to a power-law behavior for η_{PL} with an exponent close to $\beta = -1.5$, and not, as it is often assumed, to an exponential dependence. The difference is marginal as long as the defect density does not exceed $N_D = 10^{18}$ cm^{-3}, but it becomes quite pronounced for higher values of N_D. Finally, we have pointed out that TRS data may be misleading if not carefully analyzed. This is due to the fact that it is usually considered to be conclusive evidence for a competing nonradiative channel if the contribution to the decay at short times increases with increasing N_D. However, we have shown that very similar decays can be obtained without competition being involved.

ACKNOWLEDGMENT

This work was supported by the Bundesminister für Forschung und Technologie (BMFT) under Contract No. 0328327F.

[1]S. Ambros, R. Carius, and H. Wagner, J. Non-Cryst. Solids **137&138**, 555 (1991).
[2]S. D. Baranovskii, R. Hess, R. Saleh, and P. Thomas, J. Non-Cryst. Solids **137&138**, 548 (1991).
[3]M. Bort, R. Carius, and W. Fuhs, J. Non-Cryst. Solids **114**, 280 (1989).
[4]M. Bort, W. Fuhs, S. Liedtke, R. Stachowitz, and R. Carius, Philos. Mag. Lett. **64**, 227 (1991).
[5]D. K. Biegelsen, R. A. Street, and W. B. Jackson, Physica **117B&118B**, 899 (1983).
[6]S. P. Depinna and D. J. Dunstan, Philos. Mag. B **50**, 579 (1984).
[7]D. J. Dunstan, Philos. Mag. B **46**, 579 (1982).
[8]D. J. Dunstan, S. P. Depinna, and B. C. Cavenett, J. Phys. C **15**, L425 (1982).
[9]D. J. Dunstan, Philos. Mag. B **49**, 191 (1984).
[10]E. I. Levin, S. Marianer, and B. I. Shklovskii, Phys. Rev. B **45**, 5906 (1992).
[11]T. M. Searle, M. Hopkinson, M. Edmeades, S. Kalem, I. G. Austin, and R. A. Gibson, in *Disordered Semiconductors*, edited by M. A. Kastner, G. A. Thomas, and S. R. Ovshinsky (Plenum, New York, 1987), p. 357.

[12]B. I. Shklovskii, H. Fritzsche, and S. D. Baranovskii, Phys. Rev. Lett. **62**, 2989 (1989).
[13]R. Stachowitz, M. Bort, R. Carius, W. Fuhs, and S. Liedtke, J. Non-Cryst. Solids **137&138**, 551 (1991).
[14]R. Stachowitz, M. Schubert, and W. Fuhs, J. Non-Cryst. Solids **164-166**, 583 (1993).
[15]R. Stachowitz, M. Schubert, and W. Fuhs, Philos. Mag. B **70**, 1219 (1994).
[16]R. A. Street, Adv. Phys. **30**, 593 (1981).
[17]R. A. Street and D. K. Biegelsen, Solid State Commun. **44**, 501 (1982).
[18]C. Tsang and R. A. Street, Philos. Mag. B **37**, 601 (1978).
[19]C. Tsang and R. A. Street, Phys. Rev. B **19**, 3027 (1979).
[20]D. J. Dunstan, Solid State Commun. **49**, 395 (1984).
[21]F. Boulitrop and D. J. Dunstan, J. Non-Cryst. Solids **77/78**, 663 (1985).
[22]R. A. Street, J. C. Knights, and D. K. Biegelsen, Phys. Rev. B **18**, 1880 (1978).
[23]R. A. Street, Phys. Rev. B **23**, 861 (1981).
[24]M. Schubert, R. Stachowitz, R. Saleh, and W. Fuhs, J. Non-Cryst. Solids **164-166**, 555 (1993).
[25]W. B. Jackson and R. Nemanich, J. Non-Cryst. Solids **59/60**, 353 (1983).
[26]D. J. Dunstan, Philos. Mag. B **52**, 111 (1985).
[27]P. Thomas and S. D. Baranovskii, J. Non-Cryst. Solids **164-166**, 431 (1993).
[28]T. M. Searle, Philos. Mag. B **46**, 163 (1982).
[29]H. Reiss, J. Chem. Phys. **25**, 400 (1956).
[30]R. W. Collins, P. Viktorovitch, R. L. Weisfield, and W. Paul, Phys. Rev. B **26**, 6643 (1982).
[31]H. Oheda, J. Non-Cryst. Solids **164-166**, 559 (1993).
[32]R. A. Street, D. K. Biegelsen, and J. Stuke, Philos. Mag. B **40**, 451 (1979).